Acta Geochim (2021) 40(5):659–675
https://doi.org/10.1007/s11631-021-00474-2

ORIGINAL ARTICLE

Source characteristics and genesis of Sb mineralization from the Au and Sb deposits of the Youjiang Basin, SW China: constraints from stibnite trace element and isotope geochemistry

Aizat Zhaanbaeva[1,2,3] · Keqiang Peng[1] · Abiola Oyebamiji[1] · Kyiazbek Asilbekov[1]

Received: 2 November 2020 / Revised: 12 April 2021 / Accepted: 22 April 2021 / Published online: 19 May 2021

Abstract The Youjiang Basin is characterized by a wide distribution of Au and Sb deposits. These deposits are mainly hosted by sedimentary rocks from Cambrian to Triassic and are structurally controlled by faults and folds. Three types of Sb mineralization can be distinguished based on geologic characteristics, economic metals, and mineral associations. The first type is dominated by Sb mineralization but contains minor or little Au, similar to the large Qinglong deposit. The second type has a spatial association with the gold deposit but formed independent Sb mineralization, reminiscent of the Badu deposit. In the third type, Sb generally formed as an accompanying element in the Carlin-type gold deposit, and stibnite occurred as euhedral crystals filling the open space and faults in the late stage of gold mineralization, analogous to the Yata deposit. Trace element concentrations and sulfur isotopic ratio of stibnite, and oxygen isotope of stibnite bearing quartz were analyzed to infer the ore source(s) for Sb mineralization and genesis. To distinguish the various types of stibnite mineralization between the deposits, Cu, Pb, and As have recognized most diagnostic, with an elevated concentration in Au and Au-Sb deposits and depleted in Sb deposit. The $\delta^{34}S$ isotopic composition of stibnite samples from three deposits show a wide variation, ranging from −6.6 ‰ to + 17.45 ‰. Such isotopic values may indicate the sedimentary sulfur source, introduced by fluid–rock interaction. On the other hand, fluid mixing of several end members cannot be excluded. The calculated $\delta^{18}O$ isotopic data of Sb-bearing quartz show the initial ore fluid in Au and Au-Sb deposits most likely have a magmatic or metamorphic origin that enriched during fluid–rock interaction, and Sb deposit characterized by initial meteoric water. From these data, we proposed that different lithologies, fluid–rock interaction, fluid pathways, and different ore fluids controlled the compositional evolution of fluids, which might be the main reason for the diversity of Au or Sb mineralization.

Keywords Trace elements · Stable isotope · Sb mineralization · Youjiang Basin · SW China

1 Introduction

Antimony is currently recognized as a critical material for modern society. Globally, the primary production of antimony is now isolated to a few countries and is dominated by China (Anderson 2012), which supplies the world with 92% of all finished antimony products. The word antimony (from the Greek anti plus monos) means "a metal not found alone", and is seldom found in nature as a native metal because of its strong affinity for sulfur and metals such as copper, lead, and silver (Anderson 2012). Industrially, stibnite (Sb_2S_3) is the predominant ore mineral of

Supplementary Information The online version contains supplementary material available at https://doi.org/10.1007/s11631-021-00474-2.

✉ Keqiang Peng
pengkeqiang11@126.com

Aizat Zhaanbaeva
orogeny.geo@mail.ru

[1] State Key Laboratory of Ore Deposit Geochemistry, Institute of Geochemistry, Chinese Academy of Sciences, Guiyang 550081, China

[2] University of Chinese Academy of Sciences, Beijing 100049, China

[3] Institute of Geology of National Academy of Sciences of Kyrgyz Republic, Bishkek 720000, Kyrgyzstan

antimony, usually found in quartz veins and stable over a wide range of physicochemical conditions commonly encountered in nature (Williams-Jones and Normand 1997).

The Xiangzhong Sb-Au and the Youjiang Au-Sb-Hg domains, located at the southwestern part of the Yangtze Block, China, and making up the giant South China low-temperature metallogenic domain together with the Chuan-Dian-Qian Pb–Zn domain, provide over 50% of the Sb reserves of the world (Hu et al. 2017). Among these, the Sb reserves in Xiangzhong Basin has been proven to over 2.7 Mt (Peng et al. 2014), and two types of Sb deposits have been classified: independent Sb deposit occurring in the cover strata of Late Paleozoic, and Sb-Au deposit occurring in the basement (Ma et al. 2002; Hu et al. 2017), e.g. the world's largest Xikuangshan Sb and the large Woxi Au-Sb deposits, respectively.

In contrast, the Youjiang Basin is predominantly characterized by the wide distribution of Carlin-type gold deposits with proven gold reverse over 800 t (Hu et al. 2017; Su et al. 2018), and Sb commonly occurs as the accompanying element of Au in these deposits. However, several important Sb deposits are also formed in this basin, which is mainly hosted by sedimentary rocks from Cambrian to Triassic and structurally controlled by faults and folds.

Preliminary geochronological works revealed the Sb deposits or Sb mineralization in the basin are formed at 148 to 134 Ma, suggesting they shared a similar setting, and are contemporaneous with Carlin-type gold mineralization. For example, fluorite intergrown with stibnite in the Qinglong deposit has yielded Sm–Nd isochron age of 148 Ma (Peng et al. 2003). Hydrothermal quartz veins that contained variably realgar and stibnite in the Yata deposits have obtained Rb–Sr isochron age of 148 Ma (Jin 2017). Similarly, hydrothermal rutile and monazite in the Badu gold deposits have also yielded U-Th-Pb ages of 144 to 141 Ma (Gao et al. 2021).

Compared to the Carlin-type deposits in the basin, however, these low-temperature stibnite deposits have drawn much less attention (Chen et al. 2018; Li et al. 2019), the metal and fluid sources, as well as the genesis, remain controversial. Importantly, the mechanism and process resulting in the distribution of the elements, and the key factors controlling the similarity and differences of Sb mineralization, e.g. primary ore-forming fluids, physicochemical parameters, and fluid–rock interaction, remain debatable. On the other hand, the comparative studies with the Sb and Sb-Au deposits in the Youjiang Basin are scarce.

Because stibnite (Sb_2S_3) is the predominant ore mineral and shows intimate paragenesis relationships with hydrothermal quartz. Thus, we used stibnite trace element and sulfur isotope geochemistry, and oxygen isotope geochemistry of stibnite bearing quartz, from Yata Au, Badu Au-Sb, and Qinglong Sb deposits of Youjiang Basin, to clarify, the ore source for mineralization and genesis.

2 Geological background

2.1 Regional geology

The South China Block is an important metallogenic province that formed as a result of the combination of the Yangtze Craton and Cataysia Block along Jiangshao suture zone and bordered by the North China Craton from the north and Indochina Block from the west.

The Youjiang Basin covers the territory about 50,000 m^2 and becomes an important Au-As-Sb-Hg region of the southwestern part of the South China Block. It is bounded by the Mile-Shizong Fault to the northwest, the Shuicheng-Ziyun-Bama Fault to the northeast, and the Red River Fault to the southwest (Fig. 1; Hu et al. 2017). Many studies have documented that the Youjiang Basin lies on a basement of Lower Paleozoic strata and evolved into three stages, started from the passive continental margin rift basin—between Early Devonian to Early Permian, subsequent back-arc basin formation—from Late Permian to Early Triassic, followed by foreland basin formation –from Middle to Late Triassic, consistent to the opening, subduction and closing of Paleo-Tethys ocean (Zeng et al. 1995; Gu et al. 2012; Chen et al. 2015; Hu et al. 2017). The sedimentary strata are mainly composed of marine sediments with a $\sim$ 7 km thick sequence (Song et al. 2009; Galfetti et al. 2008; Yang et al. 2012). The overlying sediments from Devonian to Early Permian are mainly composed of carbonates, mudstone, sandstone, and chert.

The rifting process accompanied by strong volcanic activity occurred at the beginning of Late Permian that became a reason for the distribution of "Emeishan basalts" in the western part of the basin. Early-Middle Triassic time was described with the deposition of mudstone-sandstone turbidite and a large number of volcanic materials in the southern part of the basin (Liu et al. 1993; Feng and Bao 1994). The Youjiang Basin was closed at the end of the Middle Triassic with strong compressional deformation. Many of the former growth faults then became thrust faults. Sedimentary rocks were folded in different directions, narrow and steep folds developed in depression facies units, broad and gentle folds in platform facies units. Extraordinary strong deformation (including folding, fracturing, and faulting) occurs along the contact zone between the two facies around the isolated submarine platforms (Liu et al. 2016). Indosinian (ca. 215 Ma) and Yanshanian (ca.

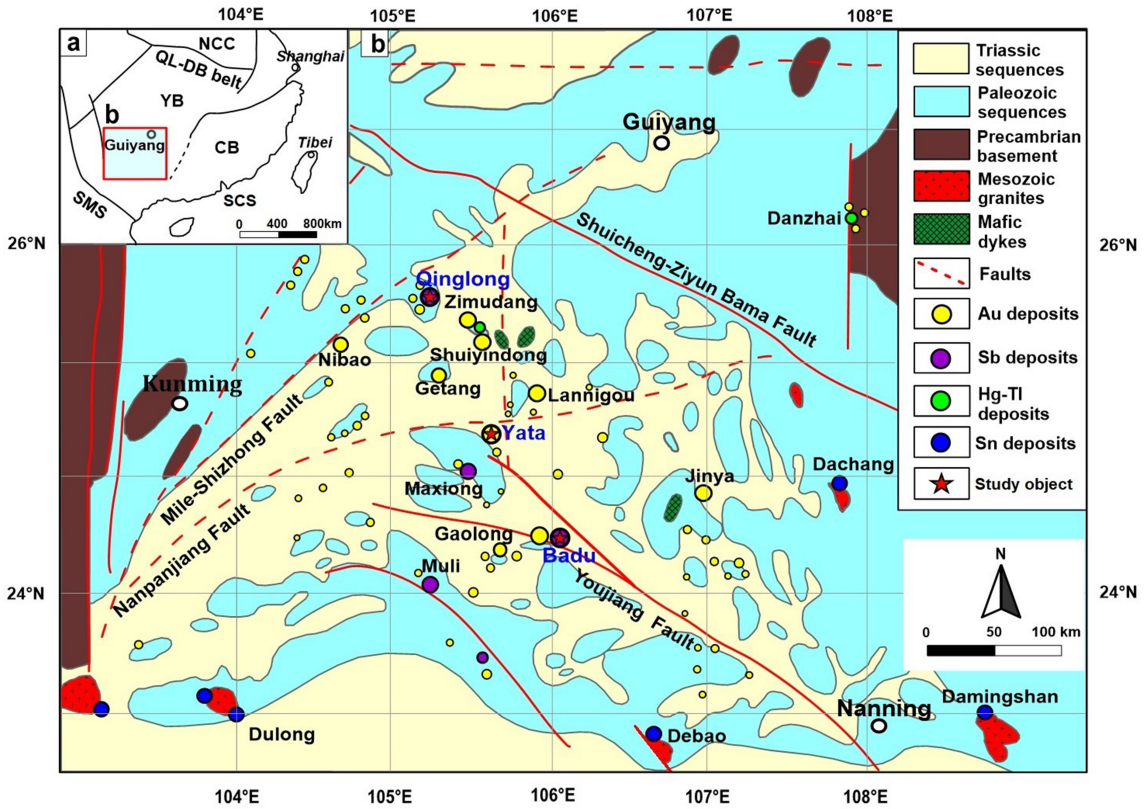

Fig. 1 Geologic map of Youjiang Basin in SW China (modified after Hu and Zhou 2012) and location of Yata, Badu, and Qinglong deposits

90 Ma) granites are distributed in the southern and eastern parts of the basin (Hu et al. 2017).

Numerous Au and Sb ore deposits, with the spatial and temporal relationship, are distributed in the Youjiang Basin. Several hundreds of Carlin-type Au deposits and occurrences have been discovered within the basin. Those deposits are hosted mainly in the Permian and Triassic strata and occur as strata-bound (Shuiyindong, Taipingdong, Zimudang, Getang, Nibao, etc.), and the fault-controlled ore deposits (Lannigou, Yata, Banqi, Zimudang, etc.; Wang et al. 2012). Antimony ore deposits occur mainly in strongly silicified limestones and brecciated claystone and siltstones near the unconformable boundaries and fault zones (Qinglong, Maxiong, etc.) and only a few Au-Sb associated ore deposits (Badu) have been found (Wang et al. 2012).

2.2 The Yata Au deposit

The Yata gold deposit is located at 15 km southwest from the Ceheng county in southwestern Guizhou (24°54′46“ N, 105°39′11” E), in the south of Nanpanjiang regional fault, on the center of Youjiang Basin, between the Badu and Qinglong deposits (Fig. 2). Before 1980, the deposit was mainly mined for arsenic (realgar) at a small scale for many years. In early 1980, the first gold mineralization was discovered, and intensive exploration by the Guizhou Bureau of Geology and Mineral Resources have been carried out and estimated more than 10 t of gold reserves (Tao et al. 1987).

The Yata deposit is hosted by the Middle Triassic Xuman Formation that is composed of siltstone, sandstone, argillaceous limestone, and shale. According to Tao et al. (1987), the Xuman Formation is divided into four members, based on the bedding thickness and grain size of the rocks. The main gold hosting strata are Member 1 and Member 2 that composed of sandstone with interbedded limestone, and sandstone and argillite, respectively. The gold mineralization occurs mainly on the southern limb of the Huangchang anticline, extending about 3 km EW along strike (Su et al. 2009). More than 40 orebodies with average gold grades from 1 to 5 g/t occur in a deposit (Han et al. 1999), and the highest detected Au grade of bulk samples is 50.7 g/t from the M1 (Zhang et al. 2003). The M1 zone is 1,500 m long, 40 to 60 m wide, and 200 m thick, with average gold grades varying from 1 to 3 g/t (Zhang et al. 2003; Su et al. 2009). The deposit is controlled by the regional EW-trending system of folds and fractures, where the main are Bajin-Huangxin and Xinluoai anticlines and Weile syncline (Tao et al. 1987; Zhang et al. 2003).

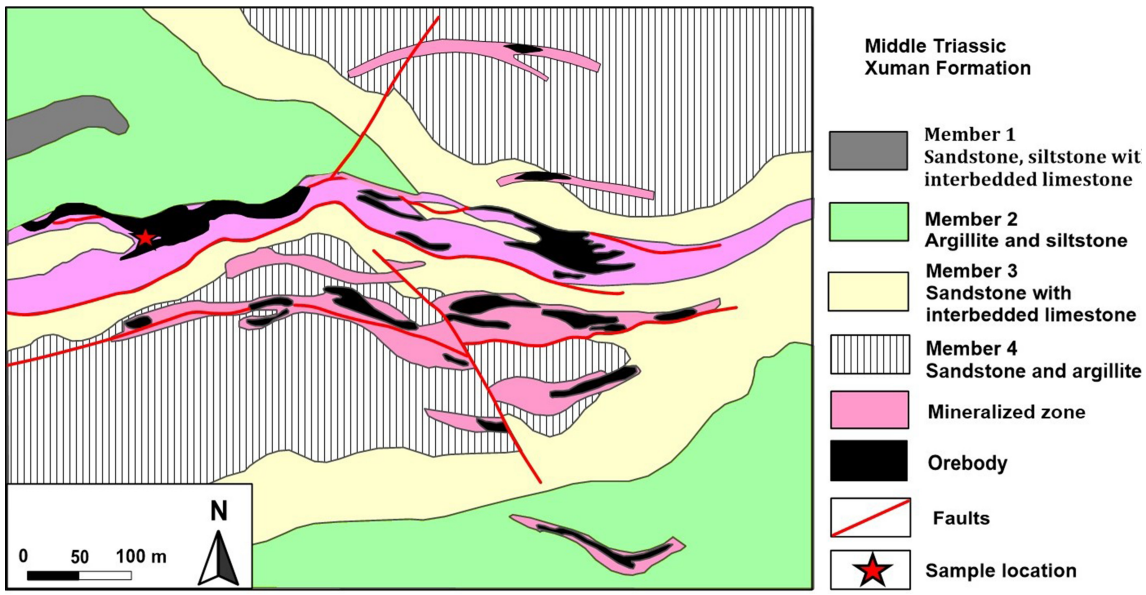

Fig. 2 Geologic map of Yata deposit (modified after Zhang et al. 2003)

Alteration is represented by decarbonatization, silicification, sulfidation, and argillization of wall-rocks and is well described in Zhang et al. (2003). Altered rocks extend far away from faults and fractures along more reactive or permeable clastic strata of calcareous shale and siltstone. Unaltered rocks contain quartz, biotite, ferroan dolomite, illite, calcite, and minor fine-grained diagenetic pyrite (Ashley et al. 1991). The ore minerals are arsenian pyrite, arsenopyrite, stibnite, marcasite, orpiment, and realgar. Gangue minerals include quartz, dolomite, calcite, and clay minerals. Stibnite (Fig. 5a) typically occurs in association with realgar and quartz across gold orebodies and has euhedral crystals filling fractures (Tao et al. 1987; Zhang et al. 2003). The ore-forming fluid of the Yata deposit is characterized by low temperature (144–263 °C) and low to moderate salinity (from 0.21 wt.% to 7.43 wt.% $NaCl_{eq}$.; Li et al. 2019). Hydrothermal quartz veins that contained variably realgar and stibnite in the Yata deposits have obtained Rb–Sr isochron age of 148 Ma (Jin 2017).

2.3 The Badu Au and Sb deposit

The Badu Au and Sb deposit located in Guanxi province, near the Youjiang regional fault (Fig. 3) at the western section of Badu anticline and have proven gold reserve of 35 t, with an average gold grade of 3 g/t (Gao 2018; Yan et al. 2018). The Badu anticline and Xilin-Baise fault-fold zones are the main structures of the deposit.

The sedimentary rocks are represented by the lower Devonian Yujiang Formation (composed of mudstone and siltstone), the Upper Devonian Liujiang Formation (comprises the interbedded sequence of silicalites and tuff with lenses of banded limestone), the Carboniferous mudstone and silicalites, the Permian rocks (interbedded limestone and silicalites, with local dolomitization and marbleization, mudstone, argillaceous sandstone, tuff intercalated with siliceous mudstone), and the lower and middle Triassic rocks (sandstone, siltstone, and mudstone; Gao 2018).

The diabase units in the Badu anticline occur as a series of arc-shaped E-W trending intrusions. The unmetamorphosed early-stage sills were emplaced into Upper Palaeozoic carbonate and clastic rocks and crop out over an area up to 20 km long and 0.5–2.0 km wide. Late-stage diabase sills are also common within sedimentary units from Devonian and Carboniferous mudstones to Lower Triassic carbonates (Qiu et al. 2017).

There are seven orebodies in a deposit that occurs as veins and tabular-shaped bodies. Most orebodies are NEE-trending with minor NW-trending and are controlled by the secondary fault systems. Gold orebodies are 20–70 m long and several meters to more than ten meters widely occur in argillaceous siltstone and altered diabase and controlled by northeast and northwest striking faults. The wall-rock alteration is described by silicification, sulfidation, calcification, and argillization. Gold occurs in arsenian pyrite and arsenopyrite crystals that widespread in averagely silicified rocks. Industrial importance has Sb mineralization that enriched in quartz veins and veinlets (Fig. 5b, c).

There are two different ore hosting rocks in a deposit, including dolerite-hosted and mudstone-hosted. The weakly altered dolerite is mainly composed of plagioclase, clinopyroxene, minor titanite and ilmenite, trace apatite, and rare sulfides and quartz, and is characterized by typical doleritic or poikilophitic texture with laths of plagioclase

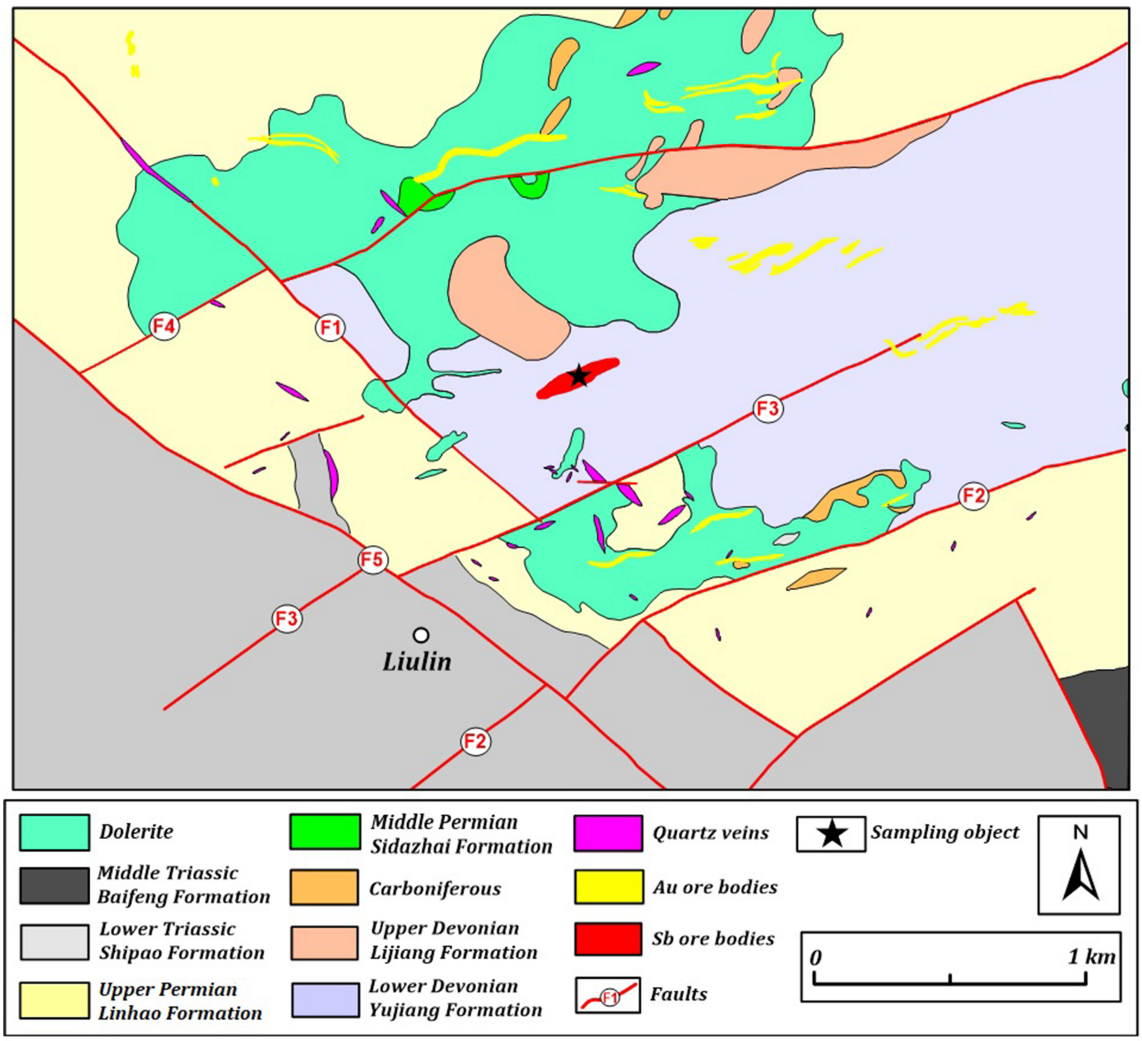

Fig. 3 Geologic map of Badu deposit (modified after Gao et al. 2021)

intergrown with clinopyroxene. Dolerite ore mineralization is represented by ankerite, sericite, pyrite, arsenopyrite, rutile, apatite, and minor base metal sulfides. Late ore stage minerals are represented by stibnite, realgar, cinnabar, and barite. Mudstone-hosted mineralization is characterized by pre-ore stage ankerite, framboidal and diagenetic pyrites; ore stage pyrite and arsenopyrite; and late ore stage stibnite, realgar, and orpiment. Fluid inclusion studies from quartz veins in altered diabase orebody are higher than in mudstone-hosted ore and show ~ 300 °C; with salinity between 5.7 wt.% and 17.5 wt.% $NaCl_{eq.}$ (Li et al. 2014). Quartz veins that typically associate with stibnite in mudstone-hosted ore show mineralization temperature between 150–280 °C. In situ SIMS U-Th-Pb dating on hydrothermal rutile and monazite yielded well consistent ages of 141.7 ± 5.8 Ma (2σ, MSWD = 1.04) and 143 ± 1.4 Ma (2σ, MSWD = 1.5), respectively, which reliably represent the mineralization age of the Badu deposit (Gao 2018; Gao et al. 2021).

2.4 The Qinglong Sb deposit

The giant Qinglong Sb deposit is in the northwestern part of the Youjiang Basin and contains eight ore blocks including, Dachang, Shuijingwan, Dishuiyan, Gulu, Houpo, Xishe, Sanwangping, and Heishanjing (Fig. 4). Among them, the Dachang ore block is the main ore hosting block. The ore bodies are typically confined to anticline structures and controlled by NE or EW striking fault systems. The deposit comprises different hosted strata including, Middle Permian Maokou Formation, Upper Permian Emeishan flood basalts, and the Longtan Formation.

The shallow-water carbonate rocks of Maokou Formation are the base for the main ore-hosting Dachang block and the middle part rocks are represented by igneous rocks and silicified limestone and the upper part is dominated by tuff and carbonaceous mudstone. The Emeishan flood

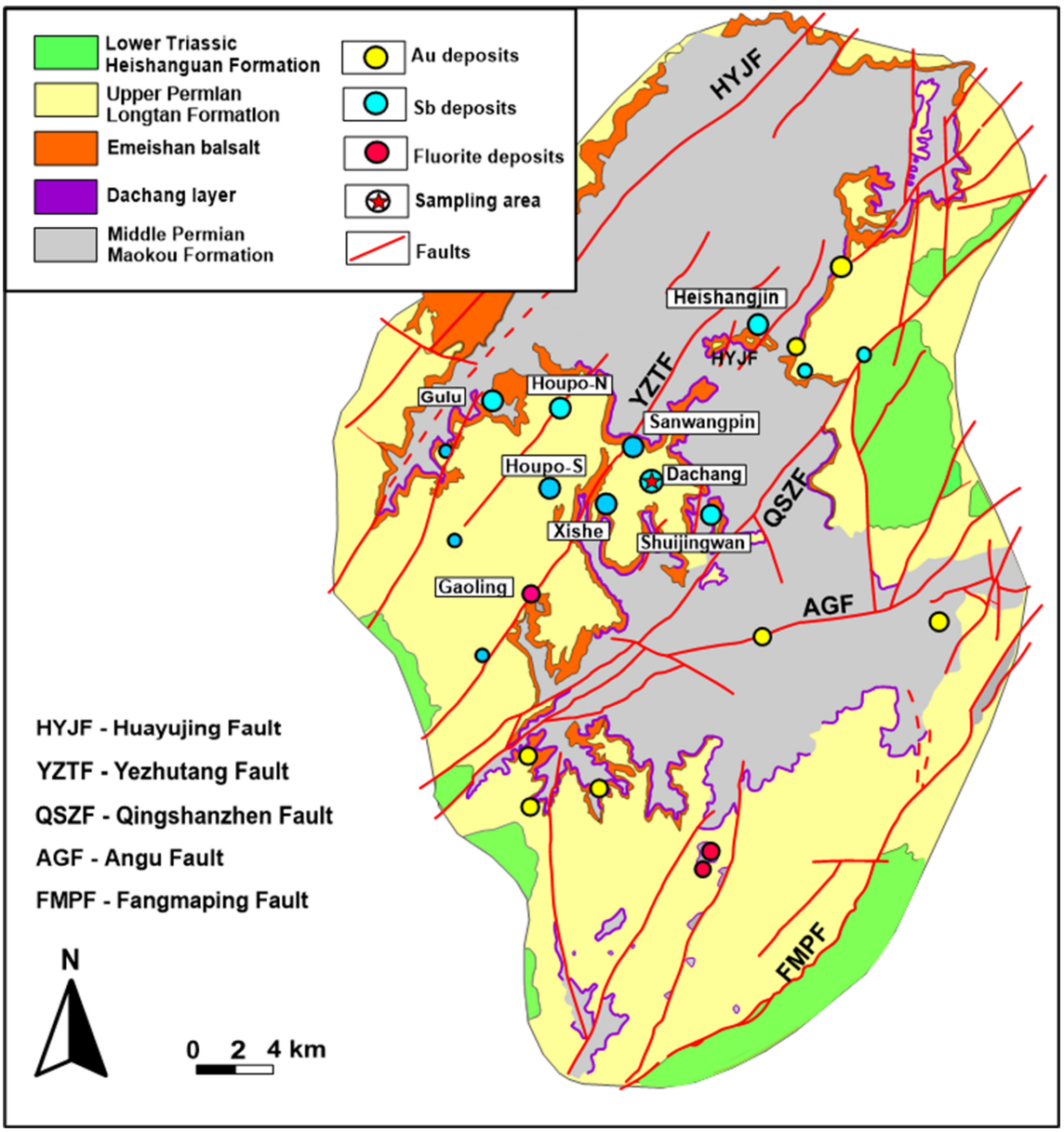

Fig. 4 Geologic map of Qinglong deposit (modified after Chen et al. 2018)

basalt is tholeiitic and the Longtan Formation is composed of sandstone and shale (Chen et al. 2014, 2018).

Dachang ore block is the SE wing of the Bihengying anticline. The ore bodies here usually have lamellar, quasi-lamellar, and lenticular forms and are divided into three units: lower, middle, and upper units (Chen et al. 2018). The host rocks of the lower unit represented by argillite and silicified limestone. The middle unit is dominated by tuff, basalt, altered and silicified limestone. Limestone is highly porous and may host quartz, stibnite, and fluorite. The upper unit is composed of tuff and carbonaceous mudstone. This unit is characterized by quartz, stibnite, and pyrite mineralization. The ore-bearing rocks are strongly altered, silicified, and locally brecciated. Early ore stage minerals are represented by Au bearing arsenian pyrite, pyrite, and quartz. That arsenian pyrite is very similar to the typical Carlin-type arsenian pyrite, with the core and rim structure. Gold mineralization with the gold grade up to 9.9 g/t developed in the Dachang layer (Chen et al. 2018). The stibnite ore stage is characterized by stibnite, pyrite, jasperoid quartz, quartz, fluorite, and kaolinite (Fig. 5d). Late ore stage minerals are quartz, calcite, orpiment, and realgar (Su et al. 2015; Li et al. 2019). Homogenization temperatures of fluid inclusions are characterized by low temperature and low-moderate salinity that range between 145–198 °C and 0.18 wt.% to 7.22 wt.% $NaCl_{eq.}$,

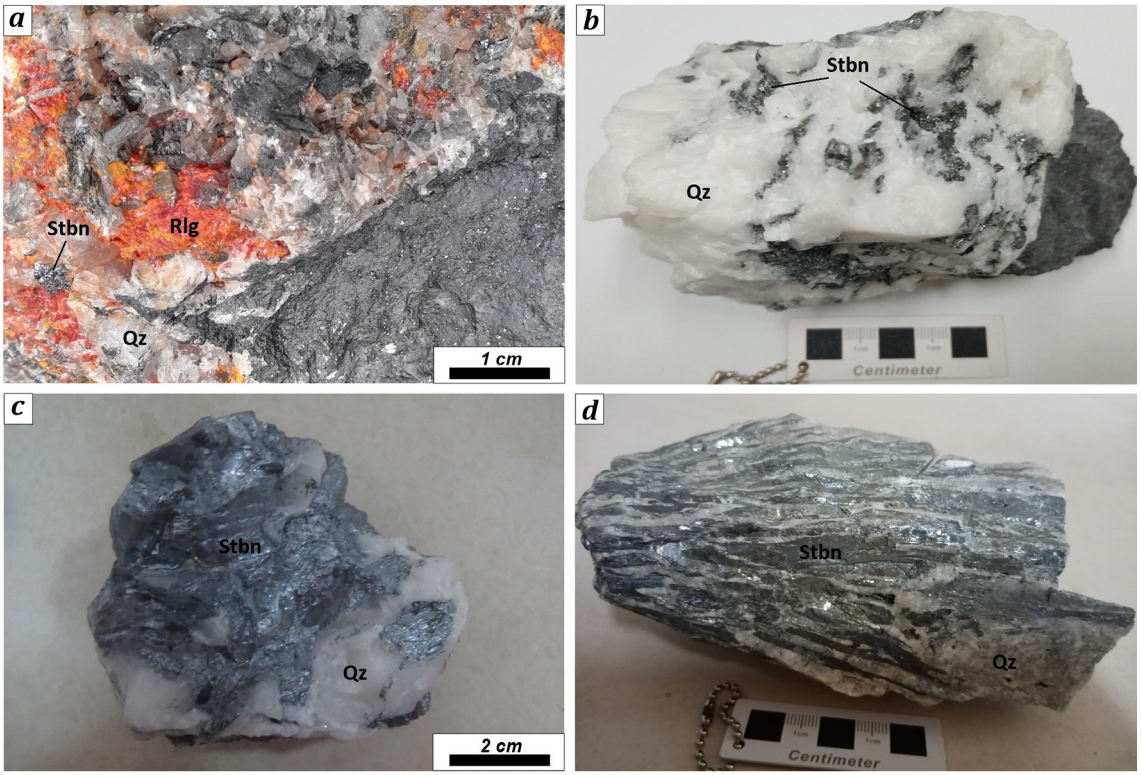

Fig. 5 Hand specimen photos; optical microscope and SEM BSE images respectively: Yata deposit (**a**); Badu deposit (**b**; **c**); Qinglong deposit (**d**)

respectively (Li et al. 2019). The Sm–Nd isotope system of stibnite bearing fluorite from Qinglong deposit corresponding to the isochron ages of 148 ± 8 Ma and 142 ± 16 Ma, suggesting late Jurassic time of ore mineralization (Peng et al. 2003).

3 Sampling and analytical methods

Stibnite samples in association with realgar and orpiment in quartz or calcite veins were collected from three different deposits. At the Yata deposit, samples were collected from the open pit. At the Badu deposit, samples were taken from underground tunnels in the mudstone-hosted zone. And at the Qinglong deposit, tunnel No. 1 and drill core samples from the Dachang ore block were collected. All representative stibnite samples were separated using a binocular microscope and analyzed for trace element, S isotope, and stibnite bearing quartz used for the O isotope.

Inductively coupled mass spectrometry (ICP-MS) technique, which is an accurate and sensitive tool with detection limits of parts-per-trillion analyzed detailed trace element characteristics in stibnite samples. After careful separation of pure stibnite from other minerals under a binocular microscope, samples were crushed with agate mortar (200 mesh) and weighed between 50–100 mg. Powdered samples later were dissolved in HNO_3 (w 5 mL) and placed on a hot plate (100 °C) overnight. Solutions were subsequently diluted to a volume of 90 mL (1% HNO_3). Trace elemental concentrations were determined on a Perkin Elmer Elan quadrupole ICP-MS. Chemical analyzes were carried out by the State Key Laboratory of Ore Deposit Geochemistry of the Institute of Geochemistry, Chinese Academy of Sciences.

Sulfur isotopic compositions were obtained from stibnite samples. Separated pure mineral grains were crushed with agate mortar (200 mesh) and weighed between 50–100 mg. The isotopic composition of sulfur expressed as $\delta^{34}S$ unit, in permil (‰), relative to Vienna Canyon Diablo Troilite (V-CDT) standard, and its analytical precision is about ± 0.3 ‰. The isotopic compositions of minerals were analyzed at the State Key Laboratory of Ore Deposit Geochemistry of the Institute of Geochemistry, Chinese Academy of Sciences.

For oxygen isotope analysis, quartz separates were crushed to 200 mesh size and degassed at 250 °C for about 2 h in Ni reaction vessels (Clayton and Mayeda 1963). Oxygen was produced by reacting 5–10 mg of quartz samples with BrF_5 and converted to CO_2 with a platinum-coated carbon rod. Oxygen isotopic compositions are expressed relative to Vienna Standard Mean Ocean Water (VSMOW) and $\delta^{18}O$ values of ore-forming fluid were

calculated from the $\delta^{18}O$ values of quartz by using isotope fractionation factors (Clayton et al. 1972). Oxygen isotopic compositions in quartz were determined using Thermo Finnigan MAT-253 Isotopic Mass Spectrometer at the Beijing Research Institute of Uranium Geology, China National Nuclear Corporation.

4 Results

4.1 Trace elements composition

Trace elements concentration in stibnite from three different deposits of the Youjiang Basin, including Yata Au and Badu Au-Sb, and Qinglong Sb deposits have been analyzed in this study. The As, Cu, Pb, V, Sr, Se, Ag, Te, Ba, Tl, Pb, and Bi elements are consistently concentrated within the stibnite in all examined samples. The full dataset is given in Appendix I and Figs. 6, 7, 8. The concentration of the elements can be high from thousands to hundreds of ppm, but most are typically tens to hundreds of ppm. A strong difference in element composition show As, Cu, and Pb between the deposits (Fig. 6).

Stibnite from Badu Au-Sb deposit characterized by elevated trace elements composition including, ***As*** ranging between 5470 to 10,900 ppm, median at 7527 ppm (n = 17); ***Cu*** varies from 267 to 2770 ppm, with the median at 874 ppm (n = 17); and ***Pb*** concentration from 1691 to 2910 ppm, with the median at 2341 ppm (n = 17); other elements have lower contents in stibnite. Stibnite samples from the Yata Au deposit also have elevated concentration of ***As***, with values from 479 to 1300 ppm, median at 737 ppm (n = 8); ***Cu*** concentration is ranging from 148 to 1481 ppm, with the mean concentration at 442 ppm (n = 8); and ***Pb*** is from 281 to 2010 ppm, with the median at 1241 ppm (n = 8). The Qinglong Sb deposit is represented by much homogeneous stibnite chemistry compare to Badu and Yata deposits, with the lowest element composition. Accordingly, Qinglong stibnite shows the following composition: ***As*** is ranging between 45 to 502 ppm, mean concentration is 242 ppm (n = 10); ***Cu*** concentration demonstrate values from 6 to 440 ppm, with the median at 74 ppm (n = 10); and ***Pb*** concentration ranges between 6.3 to 118 ppm, median at 32 ppm (n = 10) (Figs. 8, 9).

4.2 S isotopes

To investigate the source(s) of sulfur during the genesis of the Yata Au, Badu Au-Sb, and Qinglong Sb deposits, we analyzed stibnite samples. The complete isotopic dataset is provided in Appendix II and shown in Fig. 10. The measured sulfur isotopic variation of sulfides shows a wide range in $\delta^{34}S$ and extends from −6.6 ‰ to + 17.4 ‰ (Fig. 10). In more details, Badu stibnite samples show enrichment of ^{34}S and the $\delta^{34}S$ values display between + 16.56 ‰ to + 17.45 ‰, with the median of + 17 ‰ (n = 12); Yata stibnite samples have $\delta^{34}S$ values from + 5.1 ‰ to + 6.8 ‰, median at + 5.99 ‰ (n = 9); and Qinglong deposit stibnite $\delta^{34}S$ values range between −6.6 ‰ to −0.9 ‰, with the median at −3.48 ‰ (n = 26).

4.3 Oxygen isotopes

The oxygen isotopic composition of quartz may preserve a record of fluid history and is mainly influenced by the temperature and salinity of the fluid, as well as water–rock interaction (Lubben et al. 2012). Detailed $\delta^{18}O$ isotope studies for Yata and Qinglong deposits have been published earlier by Li et al. (2019), therefore, in this study, we mainly accentuate in Badu deposit and compare it with the Yata and Qinglong deposits using previous data (Appendix III; Fig. 11).

The $\delta^{18}O$ values of mineralized quartz-stibnite veins of Badu deposit vary from + 18.4 ‰ to + 20.1 ‰ (Appendix III; Fig. 11). The ore fluid temperature in the Badu deposit ranges between 150–300 °C, with an average of 230 °C (Appendix IV). The $\delta^{18}O$ values of the hydrothermal fluid are isotopically equilibrated with quartz (Matsuhisa et al. 1979). Therefore, the oxygen isotopic composition of fluid was calculated using the measured $\delta^{18}O$ values of quartz and the homogenization temperature of fluid inclusions in this mineral. We used the oxygen isotope fractionation equation for the quartz-water system given by Clayton et al. (1972): $1000\ ln\alpha\ Q\text{-}W = 3.34\ (10^6\ T\text{-}2)\text{-}3.31$.

5 Discussion

5.1 Implications from the Trace Elements in Stibnite

Results of the stibnite element chemistry allow us to recognize that stibnite from gold and antimony deposits of the Youjiang Basin tend to contain a common suite of elements, including As, Cu, Pb, V, Sr, Se, Ag, Te, Ba, Tl, Pb, and Bi (Figs. 7, 8). Among them, to distinguish various types of stibnite mineralization between the Yata Au, Badu Au-Sb, and Qinglong Sb deposits, the As, Cu, and Pb have considered most diagnostic.

Noteworthy, As is the most abundant element in stibnite samples in all three deposits Fig. 8. No visible As-bearing mineral inclusions were identified under the optical microscope and BSE SEM images (Fig. 6), suggestively As^{3+} substituted Sb^{3+} mainly as a solid solution. Despite, different crystallochemical behavior and structures of As

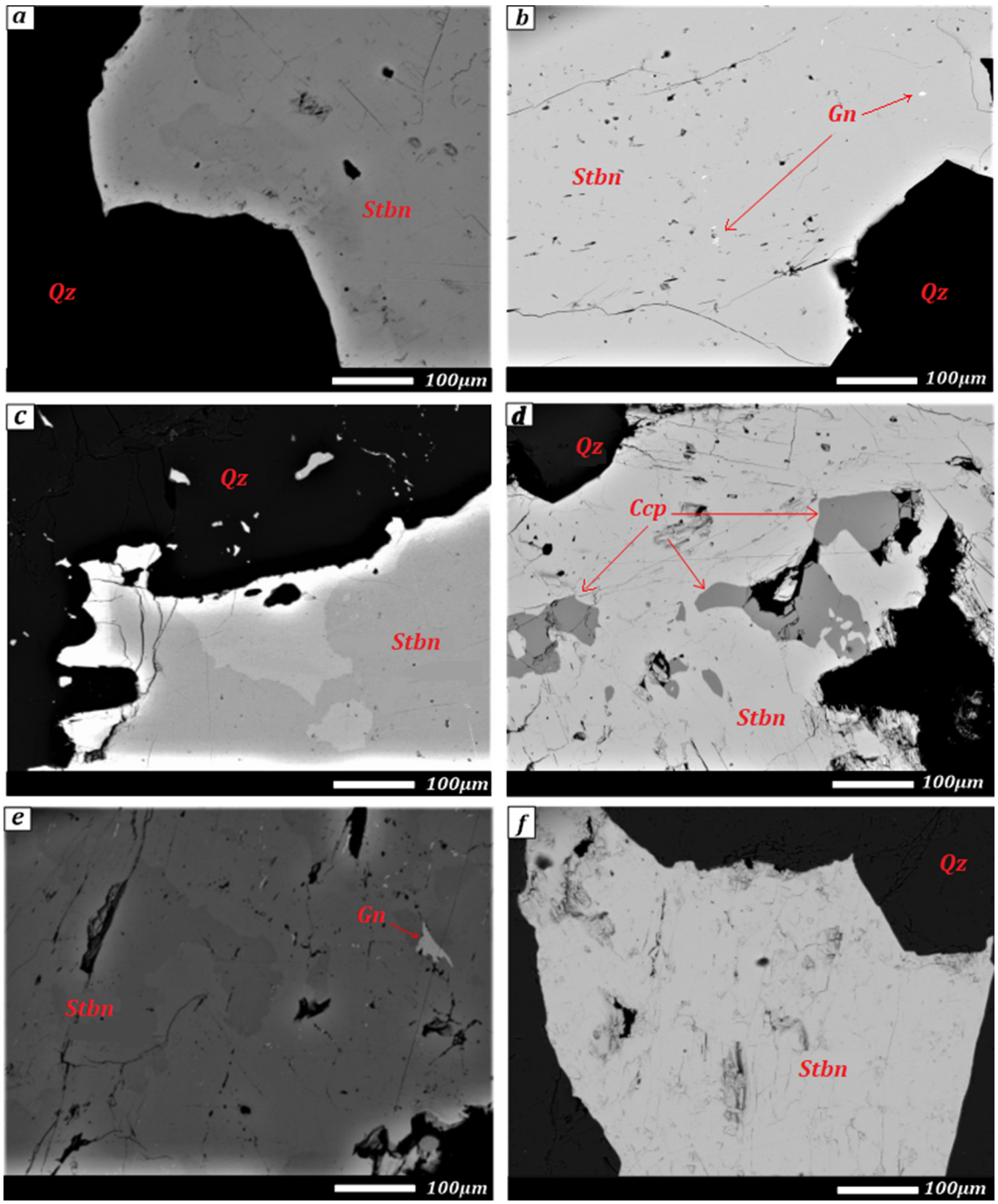

Fig. 6 SEM-BSE images of stibnite samples: **a**, **b** - Yata stibnite samples; **c**, **d**, **e** - Badu stibnite samples; **f** - Qinglong stibnite. Abbreviations: Qz-quartz; Sb-stibnite; Ccp-chalcopyrite; and Gn-galena

and Sb sulfides, they are chemically analogous elements thus resulted extensive As/Sb substitution. Such high As concentration also occurs as a solid solution in stibnite crystals from the Carlin-type gold deposits of Nevada with 1,500 to 70,000 ppm As (Dickson et al. 1975). Moreover, it is noticed that As-rich stibnite is usually enriched in Cu and Pb, compared to As-poor stibnite. Bivariate plots of As/Cu ($R^2 = 0.57$) and As/Pb ($R^2 = 0.69$) have a positive correlation (Fig. 9) and suggest that incorporating these elements is controlled by a similar process and that they are closely associated in stibnite.

The Cu and Pb content relatively less than As, but still high compare to other elements in stibnites, and more enriched in Au and Au-Sb deposits than in Sb deposits (Fig. 8). The relationships among the elements analyzed in stibnite have a positive correlation between Cu and Pb

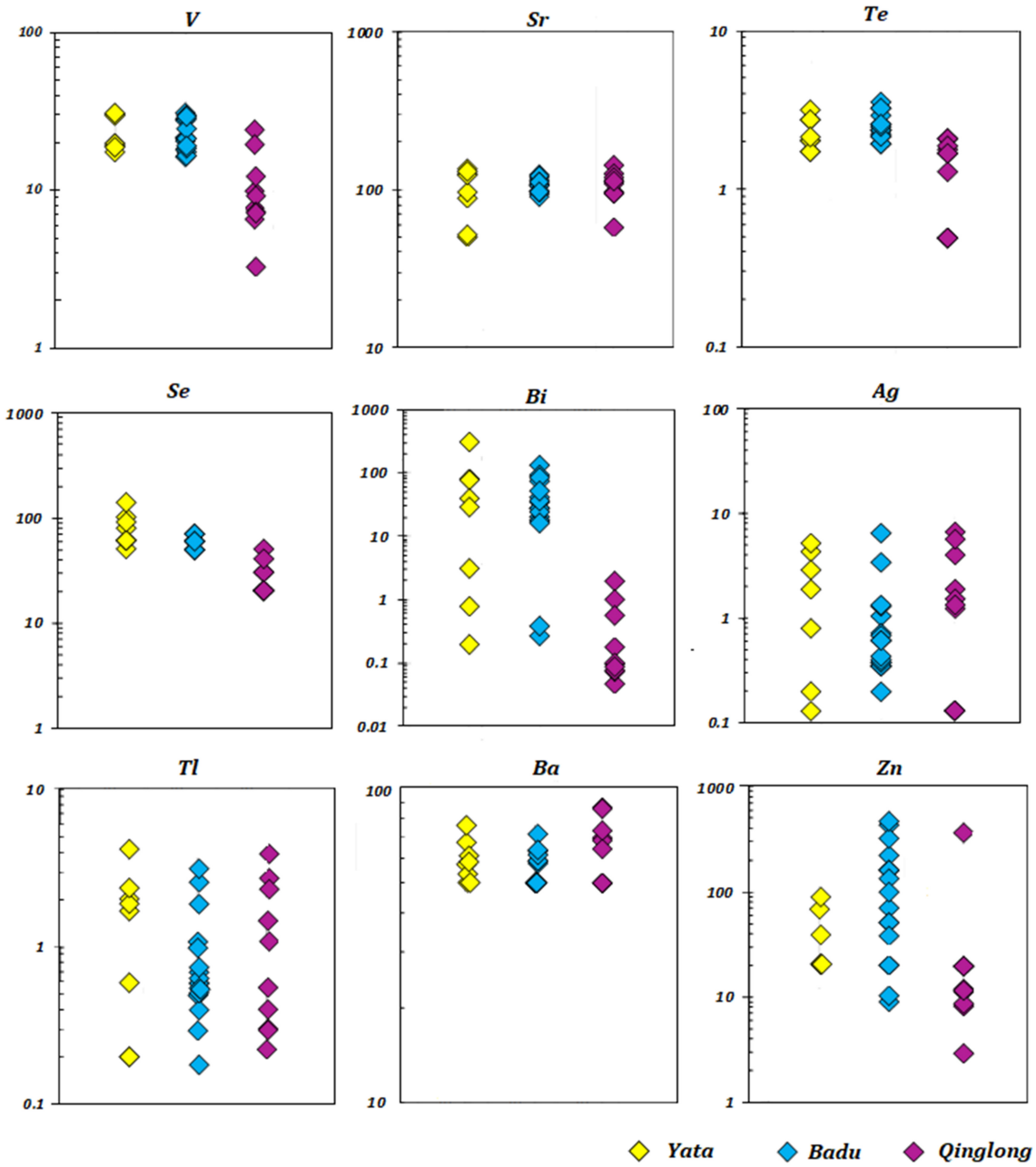

Fig. 7 Scatter plots demonstrate concentrations of V, Sr, Te, Se, Bi, Ag, Tl, Ba, and Zn elements in stibnite determined by ICP-MS (all values in ppm)

(R^2 = 0.75) element pair (Fig. 9). Suggestively, such dual inter elements positive correlation may indicate coupled incorporation in the stibnite crystal: $Sb^{3+} \leftrightarrow Cu^{+} + Pb^{2+}$ (Fu et al. 2020). Besides, BSE SEM images demonstrate Cu-bearing and Pb-bearing mineral inclusions in stibnite from Yata Au and Badu Au-Sb deposits (Fig. 6; a, b, c, d, e), except stibnite from Qinglong (Fig. 6; f). Therefore, Cu and Pb can exist as microscopic Cu-bearing and Pb-bearing mineral inclusions in stibnite, as well as structurally bound in the lattice.

Although, some mafic rocks occur in the Badu Au-Sb deposit; Qinglong Sb deposit is partially hosted by Emeishan basalts; and the hidden granitic intrusions recognized deep interior of the Youjiang Basin (Zhou 1993), undetectable or very low Rb, Cs, and Cr concentrations imply no relationship to granite or volcanic related ore fluids in the deposits. In contrast, Sr and V concentrations may indicate the result of the fluid and sedimentary rocks interaction (Jiang et al. 1999).

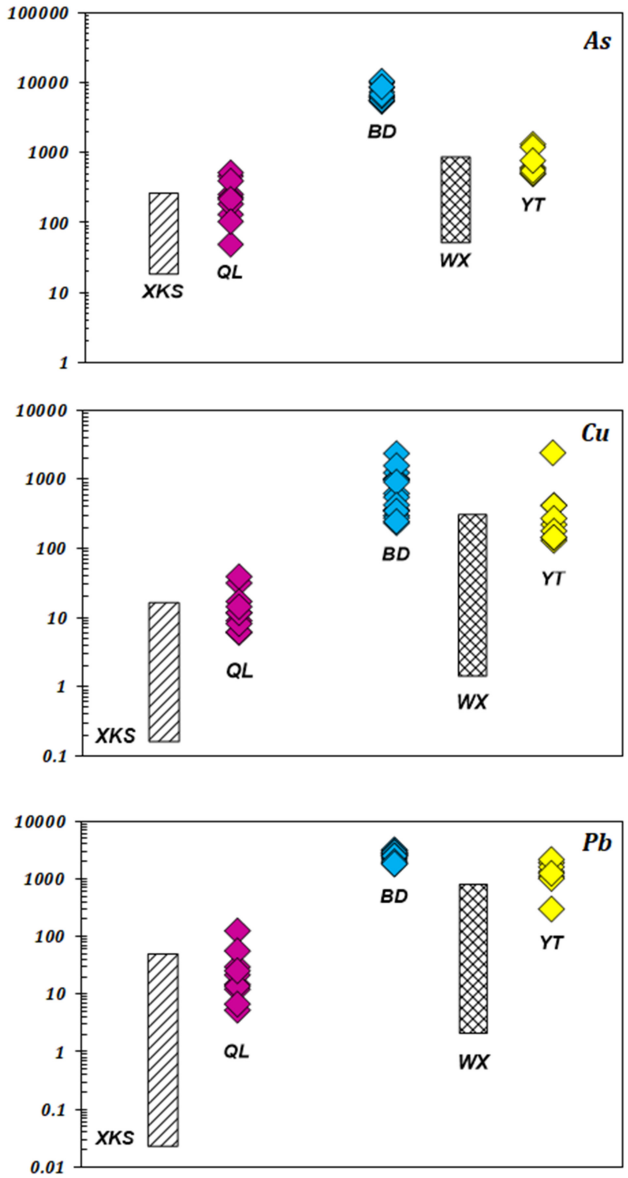

Fig. 8 Scatter plots showing the mean concentrations of key elements in stibnite determined by ICP-MS (all values in ppm). YT: Yata Au deposit, BD: Badu Au-Sb deposit, QL: Qinglong Sb deposit. For comparative purposes plotted (As, Cu, Pb) previous data for XKS: Xikuangshan Sb deposit, WX: Woxi Sb-Au-W deposit (Fu et al. 2020)

The character of stibnite trace element chemistry determines the obvious difference between the studied deposits. Accordingly, the Au and Au-Sb deposits are much enriched in triple elements association including, As, Cu, and Pb, and their concentration variability may have considered as important ore deposit type (Au or Sb) deciphering tool.

5.2 Possible Sulfur Sources

The sulfide minerals in most Au and Sb deposits of the Youjiang Basin are characterized by pyrite, stibnite, realgar, orpiment minerals, which typically form at relatively low-temperature, low fO_2, and pH-acidic to neutral conditions. Under these conditions, fractionation between aqueous sulfur and sulfides is minimal, thus the measured $\delta^{34}S$ in sulfides is approximately equal to or slightly higher than the bulk sulfur isotope compositions of sulfide-precipitating ore fluids ($\delta^{34}S_{pyrite\text{-}fluid}$ = 0 ‰–1.5 ‰; Kajiwara and Krouse 1971; Ohmoto 1972; Ohmoto and Rye 1979). In Carlin-type gold and antimony deposits of the basin, the $\delta^{34}S$ values of ore pyrite are higher than those of stibnite (Hu et al. 2002; Chen et. 2018; Yan et al. 2018). This is consistent with that ^{34}S enrichment follows the general trend $SO_{2-}{}^{4} > SO_{2-}{}^{3} > SO_{o}{}^{x} > SO^{2-}$ (Bachinski 1969; Seal 2006), and indicates that the isotopic equilibrium between sulfide and H_2S was reached.

The $\delta^{34}S$ values of stibnite from Yata Au, Badu Au-Sb, and Qinglong Sb deposits have a wide range from −6.6 ‰ to + 17.4 ‰, demonstrating both depletion and enrichment of S isotopes (Fig. 10). Among them, the Badu Au-Sb deposit exhibits the heavy $\delta^{34}S$ values (+ 16.54 ‰ to + 17.45 ‰) and is similar to diagenetic pyrite in the host rock (+ 13 ‰ to + 22 ‰; Li 2019). Such elevated sulfur values preclude any possibility of the mantle-derived source (from 0 ‰ to + 3 ‰; Chaussidon et al. 1989), implying sedimentary sulfur source, originated suggestively via fluid–rock interaction and dissolution of diagenetic pyrite. Negative sulfur values of stibnite samples from the Qinglong Sb deposit characterized by −6.6 ‰ to −0.9 ‰ (Fig. 10). Since the main host rock at Qinglong deposit is Upper Permian Emeishan flood basalts, then, the interaction between ore fluids and basaltic rocks suggestively produced sulfides with depleted $\delta^{34}S$ values. The meteoric water might have occurred during ore mineralization and also resulted in enrichment of ^{32}S in the ore-forming fluid. The $\delta^{34}S$ values of stibnite from Yata (+ 5.1 ‰ to + 6.8 ‰) are between those of the stibnite from the Badu deposit (16.54 ‰ to 17.45 ‰) and those of the stibnite from the Qinglong deposit (−6.6 ‰ to −0.9 ‰). Figure 10 shows that $\delta^{34}S$ values of the Yata stibnite similar to diagenetic pyrite (0 ‰ to + 5 ‰; Hu et al. 2002) in the host rock, also suggesting a sedimentary sulfur source.

The possible effect of the basin formation water, which is typically characterized by the heavy sulfur isotopes, because of abundant bitumen and organic components, may result from sulfate reduction to H_2S (Hu et al. 2002; Chen et al. 2015). Sedimentary wall-rocks at Yata Au, Badu Au-Sb, and partially Qinglong Sb deposits represented by Devonian to Triassic strata and the seawater

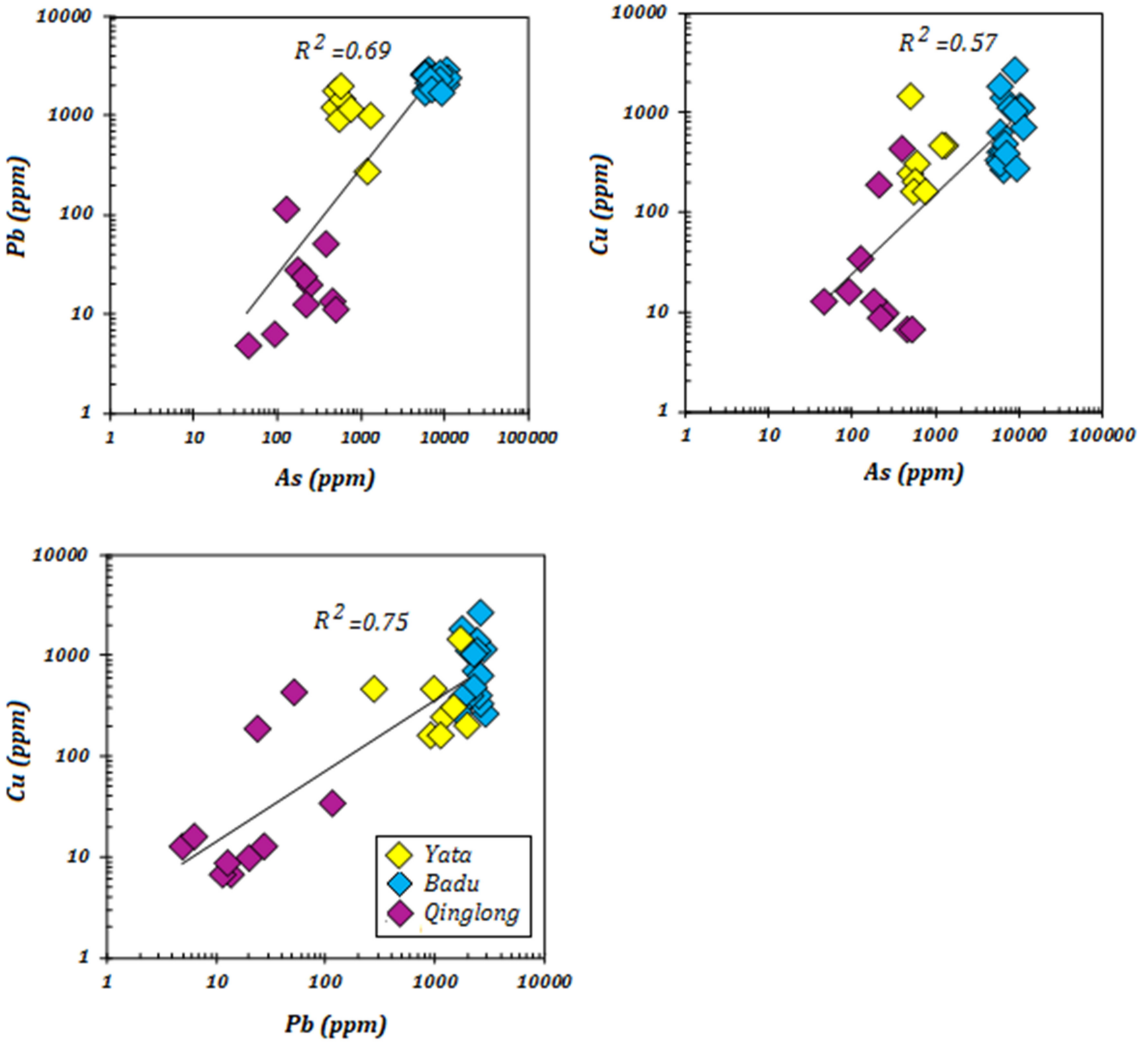

Fig. 9 Correlation plots between (**a**) As vs. Pb; (**b**) As vs. Cu; and (**c**) Cu vs. Pb elements in stibnite detected by ICP-MS

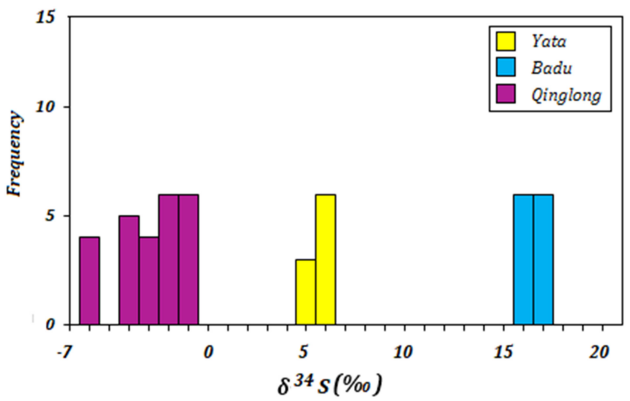

Fig. 10 Histogram of $\delta^{34}S$ values in stibnite from YT: Yata, BD: Badu, QL: Qinglong deposits

sulfate during that period range between + 30 ‰ to + 12 ‰ (Holse et al. 1997). The nature of the ore fluids mainly characterized by low-moderate temperatures, with H_2O, CO_2, and hydrocarbon components, similar to basinal fluids in the Youjiang Basin (Wang et al. 2003; Gu et al. 2010, 2012). Consequently, transportation and interaction within the host rocks at different deposits possibly resulted in dissimilar sulfur isotopes in each deposit.

However, recent in-situ sulfur isotope investigations carried out in several Carlin-type gold deposits of the Youjiang Basin suggest that magma was probably an important source of the ore-forming fluids in the basin (Hu et al. 2017). For example, in the Shuiyindong gold deposit, the $\delta^{34}S$ values for ore stage pyrite range from 2.6 ‰ to 1.5 ‰ (Hou et al. 2016), and late ore stage sulfides, such as realgar, orpiment, and stibnite range from 0.5 ‰ to 5.3 ‰ (Tan et al. 2015). Such $\delta^{34}S$ values are very close to those of mantle sulfur (0 ‰ ± 3 ‰; Chaussidon et al. 1989), suggesting a magmatic sulfur source. Also, Yan et al. (2018) noted that the $\delta^{34}S$ values of ore stage pyrite from the Lannigou gold deposit varies between 1.1 ‰ to 18.1 ‰,

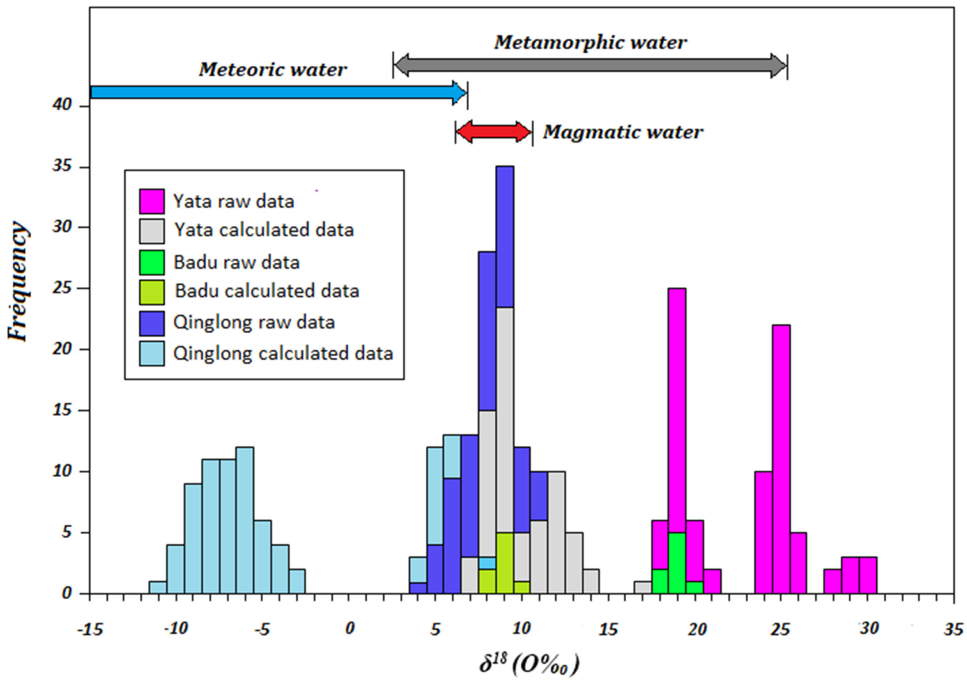

Fig. 11 Variations in (**a**) $\delta^{18}O_{quartz}$ between YT: Yata, BD: Badu, QL: Qinglong deposits and their calculated (**b**) $\delta^{18}O_{fluid}$ values. Also shown are the known ranges for the $\delta^{18}O$ isotopic compositions in meteoric, magmatic, and metamorphic water, adapted from the data in Clayton et al. (1974) and Rollinson (1993)

and the late ore stage minerals, as realgar, cinnabar, and stibnite range from 10.6 ‰ to 13.2 ‰. The author explained that the ore-bearing fluid was likely formed by the mixing of magmatic and crustal fluids. Where sulfur in the crustal fluid is suggestively derived from the sedimentary pyrite of the host rocks via fluid–rock interaction and sulfur in the magmatic fluid have mantle-derived $\delta^{34}S$ source.

Besides, Chen et al. (2015) reported a large variation of $\delta^{34}S$ values of arsenopyrites from the Carlin-type gold deposits of the Youjiang Basin and suggested sedimentary sulfur sources. And different $\delta^{34}S$ values between the deposits are a possible result of the transportation of basin formation water to the carbonate platform and variable fluid–rock interaction and meteoric water dilution.

Thus, the distinct sulfur source(s) of the gold and antimony deposits in the Youjiang Basin is still under debate and further analytical works are required to evaluate these possibilities.

5.3 Possible Oxygen Source

A variety of factors may introduce the oxygen isotope fluctuation in quartz, including fluid temperature and salinity variations, fluid boiling or immiscibility, and fluid–rock interaction (Lubben et al. 2012). The fractionation of oxygen isotopes between mineral and fluid is inversely related to temperature, and the presence of ionic salts will also affect the fractionation between water and mineral (Hoefs 1997). However, fluid inclusion microthermometry indicates that temperature and salinity of the ore fluid remained nearly constant across the stibnite ore zones, and fluid inclusion analyses have not identified fluid boiling evidence in all three deposits. The temperature variation of ~ 150 to 250 °C across the deposits, recorded by fluid inclusions, would cause variations in quartz oxygen isotope values of ~ 4 ‰ (Zheng 1993), which cannot explain the total variation in quartz oxygen isotope compositions. Thus, significant variations in fluid temperature or salinity, and the occurrence of fluid boiling seem highly unlikely to be the main cause of the variations in quartz oxygen isotope compositions measured across the deposits.

Another source for the oxygen isotope diversity of ore-stage quartz may reflect the interaction between a relatively $\delta^{18}O$ depleted ore fluid and $\delta^{18}O$ enriched carbonate host rock, as fluids migrated along different fluid-flow pathways (Rye and Bradbury 1988; Lubben et al. 2012). The origin of the $\delta^{18}O$ enrichment trend most likely is the result of the loss of an undetermined amount of H_2O vapor from the system during the ascent of the fluids. The loss of $\delta^{18}O$-depleted H_2O vapor will have the effect of enriching the remaining fluid in $\delta^{18}O$. During decarbonatization that occurs in all three deposits, oxygen likely released from sedimentary host rocks and contributes to the oxygen isotope composition of quartz precipitating from fluids flowing through these rocks (Lubben et al. 2012), causing the formation of quartz with high $\delta^{18}O$ values.

For example, in the Badu deposit, calculated $\delta^{18}O_{H2O}$ vary from + 8.52 ‰ to + 10.22 ‰ (Fig. 11; ~ 200 °C). Obtained initial $\delta^{18}O_{H2O}$ results propose two possible $\delta^{18}O$ origins: (1) magmatic water that characterized by uniform $\delta^{18}O$ values between + 5.5 ‰ to + 10 ‰, or (2) or

metamorphic water, with wide range values from + 2 ‰ to + 25 ‰ (Clayton et al. 1974). It might have suggested that the initial fluid in Badu deposit with the low $\delta^{18}O$ isotopic composition, raised to more shallow horizons and interacted with the sedimentary host rocks with a typical high isotopic composition ($\delta^{18}O_{VSMOW}$ = 24 ‰–27 ‰; Vaughan et al. 2016). Besides, the trend toward $\delta^{18}O$ enrichment at shallower levels and lower temperatures indicates that significant mixing with shallow meteoric water did not occur (Madu et al. 1990). A similar scenario likely explains the high $\delta^{18}O$ isotopic composition of ore related quartz in the Yata deposit ($\delta^{18}O_Q$ from + 18.98 ‰ to + 30.95 ‰; $\delta^{18}O_{H2O}$ from + 7.70 ‰ to + 14.87 ‰; Fig. 11), whereas, the ore is mainly hosted by sedimentary rocks that characterized by high $\delta^{18}O$ isotopic composition as mentioned before.

In contrast, at the Qinglong deposit $\delta^{18}O$ isotopic composition of the ore-related quartz and calculated fluid differ from the above two deposits. The deposit is hosted by Dachang Formation that is dominated by Emeishan basalt, or the equivalent tuff, and located along the fluid conduit between the Dachang and Maokou Formations. The $\delta^{18}O_Q$ ranges from + 4.58 ‰ to + 22.38 ‰ and $\delta^{18}O_{H2O}$ from −11.36 ‰ to + 8.74 ‰ (Fig. 9). Such values indicate fluids would subsequently become $\delta^{18}O$ depleted as a relatively $\delta^{18}O$-enriched country rock (Maokou Formation) became increasingly unavailable for reaction along fluid-flow pathways and Emeishan flood basalts and tuffs of the Dachang Formation generated decrease of $\delta^{18}O$ values; as well as considerable meteoric water dilution, might have occurred that also might result from $\delta^{18}O$ decrease.

6 Genetic model for Sb mineralization at Youjiang Basin

Youjiang Basin is an important region comprising many Carlin-type Au and Sb deposits. Their spatial–temporal distribution is related to the unique geology of the basin. Three types of Sb occurrences can be distinguished based on geologic characteristics, economic metals, and mineral associations in the Youjiang Basin including, preferentially Sb mineralization like Qinglong deposit, southwest of Guizhou. The second type has a spatial association with the gold deposit, but formed independent Sb mineralization, resembling the Badu deposit, in the northwest of Guangxi. Besides, Sb generally formed as an accompanying element in the Carlin-type gold deposit, and stibnite occurred as euhedral crystals filling the open space and faults in the late stage of gold mineralization, similar to the Yata deposit. The trace element composition of stibnites reveals As, Cu, and Pb elements as most diagnostic between the deposits. The relatively high content of these elements detected in Au-associated deposits of the Youjiang Basin, while the Sb-only deposit contains very low elements concentration. Similar characteristics are also mentioned in the Woxi Au-Sb and Xikuangshan Sb deposits of Xiangzhong Basin, South China, with the elevated concentration of As, Cu, and Pb in the Woxi Au-Sb deposit (Fu et al. 2020). Therefore, As, Cu, and Pb triple elements association is suggested as an important Sb occurrence deciphering tool in South China low-temperature deposits.

Preliminary geochronological works revealed the Sb deposits or Sb mineralization in the Youjiang Basin are formed at 148 to 134 Ma, suggesting they shared a similar setting, and are contemporaneous with Carlin-type gold mineralization. For example, fluorite intergrown with stibnite in the Qinglong deposit has yielded Sm–Nd isochron age of 148 Ma (Peng et al. 2003), hydrothermal quartz vein that contained variably realgar and stibnite in the Yata deposits have obtained Rb–Sr isochron age of 148 Ma (Jin 2017). Similarly, hydrothermal rutile and monazite in the Badu gold deposits have also yielded U-Th-Pb ages of 144 to 141 Ma (Gao et al. 2021). This age ranges coincide with the Yanshanian tectonomagmatic event in South China, from 180–87 Ma, peak at 158 Ma (Wang et al. 2012; Hu et al. 2017), that triggered the large-scale and high fluid fluxes in Youjiang Basin, as well as in other regions of the South China metallogenic domain, such as Sb mineralization in Xiangzhong Basin (Hu et al. 2017).

Generally, variations in the trace element composition of sulfides and the $\delta^{18}O$ isotopic values of fluid may be caused by changes in physicochemical fluid parameters, the availability of complex-forming ligands, boiling, as well as fluid–wall rock interaction (Huston et al. 1995; Lubben et al. 2012; Revan et al. 2014; Wohlgemuth-Ueberwasser et al. 2015; Keith et al. 2016).

In the Qinglong deposit, previous workers determined salinities of 0.18 wt.% to 7.22 wt.% $NaCl_{eq.}$ for inclusions in stibnite and intergrown quartz with homogenization temperatures ranging from ∼ 145–198 °C and CO_2-minor (Chen et al. 2018; Li et al. 2019). In the Yata deposit, the salinities similarly range from 0.21 wt.% to 7.43 wt.% $NaCl_{eq.}$, with homogenization temperatures ranging from ∼ 144–263 °C and CO_2-rich (Li et al. 2019). The Badu deposit is also characterized by low-moderate fluid inclusions homogenization temperatures ∼ 150–280 °C; CO_2-rich. From this, the ore-forming fluid of the Yata, Badu, and Qinglong deposits characterized by low-moderate temperature and moderate salinity and were stable during ore deposition (Chen et al. 2018; Li et al. 2014, 2019). The hydrothermal transport of Cu and Pb is very sensitive to boiling, which because of metal deposition, sharply reduces the concentrations of metals in the

aqueous phase (Simmons and Browne 2006), but there is no boiling among the deposits noticed.

According to Wang et al. (2003), fluids flow from the basin to the platform had taken place in the Youjiang Basin. The fluids migrated laterally and vertically through the weak horizons, faults, fractures, and paleokarst. The initial $\delta^{18}O$ values of fluids in Badu and Yata deposits are suggestively similar indicating magmatic or metamorphic origin, however, in Qinglong deposit it is more like meteoric water. Moreover, the Qinglong deposit is the best example for the fluid lateral migration, located in the platform, mainly hosted by Emeishan flood basalts and tuff, and adjacent to the primary fluid conduit. However, the Badu and Yata deposits are mainly hosted by sedimentary rocks that are rich in carbonate minerals, fluid–rock interaction caused decarbonatization and consequent $\delta^{18}O$ enrichment, and elevated elements composition, regardless of their source, while in Qinglong deposit, fluid path, less suffered host rock (basalt, tuff) influence, and meteoric water dilution suggestively resulted from $\delta^{18}O$ and trace elements decrease. Therefore, ongoing fluid circulation, meteoric water, and less wall rock influence likely played a crucial role in poor element concentration in the Qinglong deposit.

7 Conclusion

We used trace elements, S isotope studies of stibnite to characterize Sb occurrence in Au, Au-Sb, and Sb deposits of the Youjiang Basin.

1. The trace element composition of the stibnite samples from three different deposits has diverse element compositions. To distinguish the various stibnite occurrences Cu, Pb, and As have been recognized as most diagnostic. The Au and Au-Sb deposits are typically enriched in Cu, Pb, and As, while Sb deposits have very low concentrations.
2. The initial ore fluid most likely has magmatic or metamorphic origin in Badu Au-Sb and Yata Au deposits, and the water–rock interaction played an important role in these deposits' formation. However, in the Qinglong deposit, less water–rock influence and meteoric water dilution played a more important role.
3. Different lithology, fluid–rock interaction, fluid pathway, fluid flow, and meteoric water dilution were crucial during Sb occurrence in Au and Sb deposits of the Youjiang Basin.

Acknowledgements This research was funded by the National 973 Program of China (2014CB440906). We sincere thanks Yata, Badu and Qinglong Mining Companies for fieldwork support. We are especially grateful to Dong Shaohua, Hu Jing and Jing Gu for their assictence in SEM, ICP-MS and S isotope analysis, respectively.

Declarations

Conflict of interest The authors declare that there is no conflict of interest.

References

Anderson GC (2012) The metallurgy of antimony. Chem Erde 72:3–8

Ashley RP, Cunningham CG, Bostick NH, Dean WE, Chou IM (1991) Geology and geochemistry of three sedimentary-rock-hosted disseminated gold deposits in Guizhou Province, People's Republic of China. Ore Geol Rev 6:133–151

Chaussidon M, Albarède F, Sheppard SMF (1989) Sulphur isotope variations in the mantle from ion microprobe analyses of micro-sulphide inclusions. Earth Planet Sci Lett 92:144–156

Chen MH, Zhang ZQ, Santosh M, Dang Y, Zhang W (2014) The Carlin-type gold deposits of the "golden triangle" of SW China: Pb and S isotopic constraints for the ore genesis. J Asian Earth Sci 103(2015):115–128

Chen MH, Mao JW, Li C, Zhang ZQ, Dang Y (2015) Re-Os isochron ages for arsenopyrite from Carlin-like gold deposits in the Yunnan–Guizhou–Guangxi "golden triangle", southwestern China. Ore Geol Rev 64:316–327

Chen J, Yang RD, Li JD, Lu LZ, Gao JB, Lai CK, Wei HR, Yuan MG (2018) Mineralogy, geochemistry, and fluid inclusions of the Qinglong Sb-(Au) deposit, Youjiang basin (Guizhou, SW China). Ore Geol Rev 92:1–18

Clayton RN, Mayeda TK (1963) The use of bromine pentafluoride in the extraction of oxygen from oxides and silicates for isotopic analysis. Geochim Cosmochim Acta 27(1):43–52

Clayton RN, O'Neil JR, Mayeda TK (1972) Oxygen isotope exchange between quartz and water. J Geophys Res 77(17):3057–3067

Dickson FW, Radke AS, Weissberg BG, Heropoulos C (1975) Solid solutions of antimony, arsenic, and gold in stibnite (Sb_2S_3), Orpiment (As_2S_3), and realgar (As_2S_2). Econ Geol 70:591–594

Fu S, Hu R, Bi X, Sullivan NA, Yan J (2020) Trace element composition of stibnite: substitution mechanism and implications for the genesis of Sb deposits in southern China. Appl Geochem. https://doi.org/10.1016/j.apgeochem.2020.104637

Galfetti T, Bucher H, Martini R, Hochuli PA, Weissert H, Crasquin-Soleau S, Brayard A, Goudemand N, Bruhwiler T, Kuang GD (2008) Evolution of Early Triassic outer platform paleoenvironments in Nanpanjiang Basin (South China) and their significance for the biotic recovery. Sed Geol 204:36–60

Gao W (2018) Geochronology and Geodynamics of Carlin-type gold deposit in the Youjiang basin (NW Guangxi): Unpublished Ph.D. dissertation, Guiyang, China, Institute of Geochemistry, Chinese Academy of Sciences (in Chinese with English abs)

Gao W, Hu RZ, Hofstra A, Li QL, Zhu JJ, Peng KQ, Mu L, Huang Y, Ma JW, Zhao Q (2021) U-Pb dating on hydrothermal rutile and monazite from the badu gold deposit supports an early cretaceous age for carlin-type gold mineralization in the Youjiang Basin Southwestern China. Econ Geol. https://doi.org/10.5382/econgeo.4824

Gu XX, Zhang YM, Li BH, Dong SW, Xue CJ, Fu SH (2012) Hydrocarbon and ore bearing basinal fluids: a possible link between gold mineralization and hydrocarbon accumulation in the Youjiang Basin, South China. Mineral Deposit 47:663–682

Han ZJ, Wang YG, Feng JZ, Chen TJ, Luo XH, Liu YH (1999) The geology and exploration of gold deposits in southwestern

Guizhou, China. Guizhou Science and Technology Press, Guizhou, pp 1–146 (**in Chinese with English abs**)

Hou L, Peng HJ, Ding J, Zhang JR, Zhu SB, Wu SY, Wu Y, Ouyang HG (2016) Textures and in situ chemical and isotopic analyses of pyrite, Huijiabao Trend, Youjiang Basin, China: implications for paragenesis and source of sulfur. Econ Geol 111:331–353. https://doi.org/10.2113/econgeo.111.2.331

Hu RZ, Su WC, Bi XW, Tu GZ, Hofstra AH (2002) Geology and geochemistry of Carlin-type gold deposits in China. Mineral Deposita 37(37):378–392

Hu RZ, Fu SL, Huang Y, Zhou MF, Fu SH, Zhao CH, Wang YJ, Bi XW, Xiao JF (2017) The giant South China Mesozoic low-temperature metallogenic domain: reviews and a new geodynamic model. J Asian Earth Sci 137:9–34

Huston DL, Sie SH, Suter GF, Cooke DR, Both RA (1995) Trace elements in sulfide minerals from eastern Australian volcanic-hosted massive sulfide deposits; Part I, Proton microprobe analyses of pyrite, chalcopyrite, and sphalerite, and Part II, Selenium levels in pyrite; comparison with delta 34S values and implications for the source of sulfur in volcanogenic hydrothermal systems. Econ Geol 90:1167–1196

Jiang SY, Han F, Shen JZ, Palmer MR (1999) Chemical and Rb–Sr, Sm–Nd isotopic systematic of tourmaline from the Dachang Sn-polymetallic ore deposit, Guangxi Province, P.R. China. Chem Geol 157:49–67

Jin XY (2017) Geology, mineralization and genesis of the Nibao, Shuiyindong and Yata gold deposits in SW Guizhou province, China PhD thesis. China University of Geosciences, Wuhan, pp, 1–150 (in Chinese with English abstract)

Keith M, Haase KM, Klemd R, Krumm S, Strauss H (2016) Systematic variations of trace element and sulfur isotope compositions in pyrite with stratigraphic depth in the Skouriotissa volcanic-hosted massive sulfide deposit, Troodos ophiolite. Cyprus Chem Geol 423:7–18

Li JX (2019) Study on the metallogenic source and the fluid evolution of the Carlin-type gold deposits, a case study of in-situ sulfur isotopes and trace elements of pyrites of gold deposits from two sedimentary facies in the Youjiang Basin. Unpublished Ph.D. dissertation, Guiyang, China, Institute of Geochemistry, Chinese Academy of Sciences (in Chinese with English abs)

Li PR, Pang BC, Wang BH, Li YQ, Zhou YQ, Lv JW, Ma JJ (2014) Fluid inclusions and rare earth elements of the badu gold deposit Guangxi China: implications for mineralization. Acta Geol Sin - English Ed 88:1118–1119. https://doi.org/10.1111/1755-6724.12379_29

Li J, Hu R, Xiao J, Zhuo Y, Yan J, Oyebamiji A (2019) Genesis of gold and antimony deposits in the Youjiang metallogenic province, SW China: evidence from in situ oxygen isotopic and trace element compositions of quartz. Ore Geol Rev. https://doi.org/10.1016/j.oregeorev.2019.103257

Liu XJ, Liang QD, Li ZI, Castillo PR, Shi Y, Xu JF, Huang XL, Liao S, Huang WL, Wu WN (2016) Origin of Oermian extremely high Ti/Y mafic lavas and dykes from western Guanxi, SW China: implications for the Emeishan mantle plume magmatism. J Asian Earth Sci 141:97–111

Lubben JD, Cline JS, Barker SLL (2012) Ore fluid properties and sources from quartz associated gold at the Betze-Post Carlin-type gold deposit, Nevada, United States. Econ Geol 107:1351–1385

Ma DS, Pan JY, Xie QL, He J (2002) Ore source of Sb (Au) deposits in Center Hunan: I. Evidences of trace elements and experimental geochemistry. Mineral Deposits 3:366–376 (**in Chinese with English abstract**)

Matsuhisa Y, Goldsmith J, Clayton R (1979) Oxygen isotopic fractionation in the system quartz-albite-anorthite-water. Geochim Cosmochim Acta 43:1131–1140

Ohmoto H, Rye RO (1979) Isotopes of sulfur and carbon. In: Barnes HL (ed) Geochemistry of hydrothermal ore deposits, 2nd edn. Wiley, New York, pp 509–567

Peng JT, Hu RZ, Jiang GH (2003) Samarium-Neodymium isotope system of fluorites from the Qinglong antimony deposit, Guizhou Province: constraints on the mineralizing age and ore-forming materials' sources. Acta Petrol Sin 19:785–791 (**in Chinese with English abstract**)

Peng YW, Gu XX, Zhang YM, Liu I, Wu CY, Chen SY (2014) Ore-forming process of the Huijiabao gold district, southwestern Guizhou Province, China: evidence from fluid inclusions and stable isotopes. J Asian Earth Sci 93:89–101

Qiu L, Yan DP, Yang WX, Wang JB, Tang XL, Ariser S (2017) Early to Middle Triassic sedimentary records in the Youjiang Basin, South China: implications for Indosinian orogenesis. J Asian Earth Sci 141:125–139. https://doi.org/10.1016/j.jseaes.2016.09.020

Revan MK, Genc Y, Maslennikov VV, Maslennikov SP, Large RR, Danyushevsky LV (2014) Mineralogy and trace-element geochemistry of sulfide minerals in hydrothermal chimneys from the Upper-Cretaceous VMS deposits of the Eastern Pontide orogenic belt (NE Turkey). Ore Geol Rev 63:129–149

Rollinson HR (1993) Using geochemical data: evaluation, presentation, interpretation. Longman Scientific & Technical, Copublished in the U.S. with Wiley, New York

Seal RR (2006) Sulfur isotope geochemistry of sulfide minerals. Rev Min Geochem 61(1):633–677

Simmons SF, Brown KL (2006) Gold in magmatic hydrothermal solutions and the rapid formation of a giant ore deposits. Science 314(5797):288–291. https://doi.org/10.1126/science.1132866

Song CA, Feng ZH, Lei LQ (2009) Geotectonic metallogenic evolution and belt of Tin polimetal ore and exploration in Guanxi. J Guiylin Univ Technol 29:207–215 (**in Chinese with English abstract**)

Su WC, Hu RZ, Xia B, Xia Y, Liu YP et al (2009) Calcite Sm-Nd isochron age of the Shuiyindon Carlin-type gold deposit, Guizhou, China. Chem Geol 258:269–274

Su WC, Zhu LY, Ge X, Shen NP, Zhang XC, Hu RZ (2015) Infrared microthermometry of fluid inclusions in stibnite from the Dachang antimony deposit, Guizhou. Acta Petrol Sin 31(4):918–924 (**in Chinese with English abstract**)

Su WC, Dong WD, Zhang XC, Shen NP, Hu RZ, Hofstra AH, Cheng LZ (2018) Carlin-type gold deposits in the Dian-Qian-Gui "Golden Triangle" of Southwest China. Rev Econ Geol 20:157–185

Tan QP, Xia Y, Xie ZJ, Yan J, Wei DT (2015) S C O H and Pb isotopic studies for the Shuiyindong Carlin-type gold deposit Southwest Guizhou China: constraints for ore genesis. Chin J Geochem 34(4):525–539. https://doi.org/10.1007/s11631-015-0063-5

Tao CG, Liu JS, Dan G (1987) Geological characteristics and genesis of Yata gold deposit, Ceheng county. Geol Guizhou 4:135–150 (**in Chinese**)

Vaughan JR, Hickey KA, Barker SL (2016) Isotopic chemical and textural evidence for pervasive calcite dissolution and precipitation accompanying hydrothermal fluid flow in low-temperature carbonate-hosted gold systems. Econ Geol 111:1127–1157. https://doi.org/10.2113/econgeo.111.5.1127

Wang G, Hu RZ, Su WC, Zhu LM (2003) Fluid flow and mineralization of Youjiang Basin in the Yunnan-Guizhou-Guangxi area, China. Sci China (Series D) 46:99–109

Wang YJ, Wu CM, Zhang AM, Fan WM, Zhang YH, Zhang YZ, Peng TP, Yin CQ (2012) Kwangsian and Indosinian reworking of the eastern South China Block: constraints on Zircon U-Pb geochronology and metamorphism of amphibolite and granulite. Lithos 150:227–242. https://doi.org/10.1016/j.lithos.2012.04.022

Williams-Jones AE, Normand C (1997) Controls of mineral paragenesis in the system Fe-Sb-S-O. Econ Geol 92:308–324

Wohlgemuth-Ueberwasser CC, Viljoen F, Petersen S, Vorster C (2015) Distribution and solubility limits of trace elements in hydrothermal black smoker sulfides: an in-situ LA-ICP-MS study. Geochim Cosmochim Acta 159:16–41. https://doi.org/10.1016/j.gca.2015.03.020

Yan J, Hu RZ, Liu S, Lin YT, Zhang JC, Fu SL (2018) NanoSIMS element mapping and sulfur isotope analysis of Au-bearing pyrite from Lannigou Carlin-type Au deposit in SW China: new insights into the origin and evolution of Au-bearing fluids. Ore Geol Rev 9229–9241. https://doi.org/10.1016/j.oregeorev.2017.10.015

Yang JH, Cawood PA, Du YS, Huang H, Hu LS (2012) Detrital record of Indosinian mountain building in SW China: provenance of the Middle Triassic turbidites in the Youjiang Basin. Tectonophysics 574–575:105–117. https://doi.org/10.1016/j.tecto.2012.08.027

Zeng YF, Liu WJ, Cheng HD, Zheng RC, Zhang JQ, Li XQ, Jiang TC (1995) Evolution of sedimentation and tectonics of the Youjiang composite basin, south China. Acta Geol Sin 69:113–124 (**in Chinese with English abstract**). https://doi.org/CNKI:SUN:DZXW.0.1995-04-001

Zhang XC, Spiro B, Halls C, Stanley C, Yang KY (2003) Sediment hosted disseminated gold deposits in southwest Guizhou, PRC: their geological setting and origin in relation to mineralogical, fluid inclusion, and stable-isotope characteristics. Int Geol Rev 45:407–470